Assessing Gas-Phase Ion Reactivity of 50 Elements with NO and the Direct Application for ^{239}Pu in Complex Matrices Using ICP-MS/MS

Kirby P. Hobbs, Amanda D. French,* Kali M. Melby, Eric J. Bylaska, Khadouja Harouaka, Richard M Cox, Isaac J. Arnquist, and Chelsie L. Beck

ABSTRACT: Understanding the reactivity of metal cations with various reaction gases in inductively coupled plasma tandem mass spectrometry (ICP-MS/MS) is important to determine the best gas to use for a given analyte/interference pair. In this study, nitric oxide (NO) was investigated as the reaction gas following previous experimental designs. The reactions with 50 elements were investigated to examine periodic trends in reactivity, validate theoretical modeling of reaction enthalpies as a method to screen reactant gases, and provide a baseline data set for potential in-line gas separation methods. ICP-MS/MS studies involving actinides are typically limited to Th, U, and Pu, with analyses of Np and Am rarely reported in the literature. To date, only two previous methods have investigated the use of NO in ICP-MS/MS analyses. To showcase the utility of NO, a method was developed to measure ^{239}Pu in the presence of environmental matrix constituent and other actinides, like what could be expected from postdetonation debris, with no chemical separation prior to analysis. $^{239}Pu^+$ was reacted to form $^{239}Pu^{16}O^+$, eliminating interferences derived from the sample matrix by measuring the $^{239}Pu^+$ intensity at m/z = 255 ($^{239}Pu^{16}O^+$). To validate NO for $^{238}U^1H^+$ interference removal in environmental matrices, standard reference materials were diluted to 1 mg/g of solution and spiked to 0.05 pg/g of ^{239}Pu and 1 μg/g ^{238}U (Pu/U = 5 × 10^{-8}). Measured ^{239}Pu concentrations were within 6% of the spiked value. These results demonstrate that reliable ^{239}Pu measurements can be made at levels relevant to nuclear forensics without the need for extensive chemical matrix separation prior to analysis.

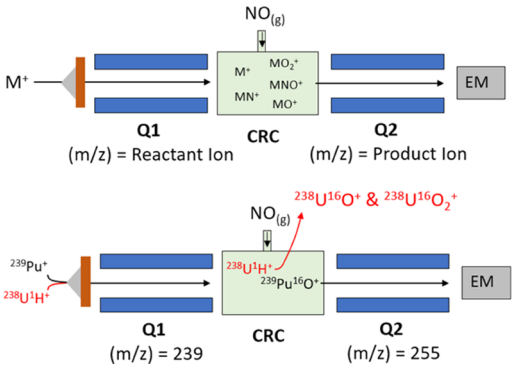

Inductively coupled plasma tandem mass spectrometry (ICP-MS/MS) has become a highly valued technique due to its effectiveness at removing matrix- and plasma-derived polyatomic and isobaric interferences (e.g., $^{87}Rb^+$ on $^{87}Sr^+$, $^{184}W^{16}O_3^+$ on $^{232}Th^+$).[1−4] ICP-MS/MS utilizes a collision/reaction cell (CRC) positioned between two mass filters, where all ions of the same mass-to-charge ratio (m/z) are introduced into the CRC and are separated on the basis of differences in gas-phase ion−molecule reactivities. This technique allows in-line analyte/interference separation, decreasing or removing time-intensive sample preparation that may hamper the analysis of time-sensitive samples. To fully utilize ICP-MS/MS, a systematic understanding of ion reactivity with a variety of reaction gases in the CRC is necessary to resolve potential isobaric and polyatomic interferences. Previous investigations of O_2, NH_3, CH_3F, N_2O, H_2S, CO_2, and OCS (O═C═S) have indicated selective product ion formation across the periodic table that can be tailored for specific analyses.[5−12] For some of these systems, we have shown that knowledge of a reaction enthalpy, which was calculated using density functional theory (DFT), is sufficient to predict the general reactivity of an ion with a given reaction gas. This approach has an accuracy of >85%.[5,6,11] Note that the ICP source creates ion populations at elevated temperatures so that appreciable excited state populations may exist, and changes to source conditions may change observed product ratios. A more detailed discussion of excited state behavior is available in previous work.[5,13,14] Nevertheless, general knowledge of ground state reaction enthalpies through these DFT calculations can be leveraged to choose an appropriate reaction partner that can subsequently be optimized to separate a given analyte/interference pair.

Several fundamental ion−molecule studies have been conducted with nitric oxide (NO), e.g., utilizing selected ion flow tube-mass spectrometry (SIFT-MS),[15,16] guided ion beam tandem mass spectrometry (GIBMS),[17−19] and Fourier transform ion cyclotron resonance mass spectrometry (FTICR)-MS.[20−23] These experiments have primarily shown monoxide and dioxide products with charge transfer (i.e., M^+ +

NO → M + NO^+) occurring for many elements.[15−17] While there are known differences between these applications and ICP-MS/MS analyses (see Supporting Information for more detail), these experiments provide an understanding of general gas-phase ion reactivity that can also provide a basis to determine the expected reactions in ICP-MS/MS.[5,6,11] We selected NO as the reaction gas as it parallels other oxide-forming gases (e.g., N_2O, O_2, CO_2) used for ICP-MS/MS analyses but has been far less researched for this application.[24] The larger bond dissociation energy (BDE) for NO (6.5 eV) means it would be more discriminating than that for O_2 (5.2 eV) as a reaction gas. These characteristics make it potentially beneficial to actinide applications.[20−25]

Prior to the development of the CRC for use in ICP-MS, plutonium is needed to be purified with chemical separation to avoid interferences from matrix constituents (e.g., $^{238}U/^{238}Pu$, $^{239}Pu/^{238}U^1H$, $^{207}Pb^{16}O_2$, $^{241}Am/^{241}Pu$, etc.) prior to analysis.[26−29] Such upfront chemistry is time-consuming and involves additional steps, which may also reduce recovery or introduce contamination. Advances in tandem MS capabilities may allow for analyses without initial sample processing. Prior work has primarily focused on removing $^{238}U^1H^+$ from $^{239}Pu^+$ using He, O_2, CO_2, NO, and He/NH_3 in the CRC.[24,25,30−34] Additional work has shown that the molarity of the nitric acid in the sample solution and the use of a membrane desolvation system can reduce hydride formation by another order of magnitude.[31,35,36] These methods have been optimized for environmental samples, which typically contain less than 10 μg/g total U and less than 1 pg/g Pu. There has even been successful separation between ^{238}U and ^{238}Pu of ratios up to 4000 U/Pu in purified Pu and U standards[37] that show potential for ICP-MS/MS to remove enough ^{238}U for accurate ^{238}Pu determinations. It is important to note that these developed methods still require the need for chemical separations due to the low concentration of Pu in environmental samples. However, postdetonation debris from a nuclear event is expected to mix with environmental material.[38] This results in a complex sample matrix that contains elevated levels of actinides from the device in the presence of high levels of elements that are ubiquitous in the environment (e.g., Fe, Ca, Pb, Th, U, etc.).

In this work, NO was investigated as a reaction gas for a broad suite of elements following a similar experimental model to previously investigated gases N_2O, CO_2, and OCS[5,6,11] with, in this study, the addition of actinides (Th, Np, U, Pu, and Am). DFT was utilized to calculate reaction enthalpies that predict whether a reaction would occur at the expected ion energy for each ion analyte. Unique to this work is that the DFT approach was used to determine that NO would be a suitable reaction gas to analyze ^{239}Pu with high concentrations of ^{238}U present in the sample, where $^{238}U^1H^+$ is formed in the plasma. Consequently, this top-down approach is demonstrated by utilizing NO reaction gas to examine the in-line separation of $^{238}U^1H^+$ from the analyte ion $^{239}Pu^+$ with no prior chemical separation. Examples of ^{239}Pu analysis in solutions containing various concentrations of ^{238}U are provided. The method was verified with the analysis of ^{239}Pu and ^{238}U spiked and unspiked standard reference materials (NIST SRM 4350b, NIST SRM 3454, NIST SRM 2711a).

METHODS

Reagents and Materials. The fundamental ion−molecule reaction experiment was conducted using a custom 1 ng/g multielement (ME) standard, which was made from 1000 μg/g stock standards (Inorganic Ventures; Christiansburg, VA) containing Be, B, Mg, Al, K, Ca, V, Cr, Mn, Fe, Co, Ni, Cu, Zn, Ga, As, Se, Rb, Sr, Mo, Pd, Ag, Cd, In, Cs, Ba, La, Ce, Pr, Nd, Sm, Eu, Gd, Dy, Ho, Er, Tm, Yb, Lu, W, Ir, Pt, Au, Tl, and Pb. Nitric oxide (99.5% purity; Advanced Specialty Gases; Reno, NV) was used as the reaction gas. For the actinide application, standard solutions were made from stock Th, U (Inorganic Ventures; Christiansburg, VA), Pu (NBL-CRM-128), ^{237}Np, and ^{243}Am (Eckert & Ziegler Isotope Products; Valencia, CA) standards. All standards were diluted with 2% HNO_3 (optima grade; Fisher Scientific; Pittsburgh, PA) and 18.2 MΩ·cm deionized water. A 2% HNO_3 solution was used as a blank.

For the actinide measurements, single-element standards of Pu (0.5 pg/g) and U (10, 100, and 300 ng/g) were made for instrument optimization and to test backgrounds derived from a high U matrix. Multielement standards of U and Pu were prepared with the concentration of ^{238}U ranging from 1 to 5000 ng/g, while ^{239}Pu concentrations ranged from 0.05 to 0.5 pg/g. This resulted in ^{239}Pu: ^{238}U ratios from 10^{-4} to 10^{-8}. To determine the accuracy of this method, NIST SRMs were dissolved and diluted to 1 mg of standard per gram of solution. The reference materials used consist of the following: river sediment materials collected from the Colombia River near Hanford, WA (NIST SRM 4350b); lake sediment material collected near the Chalk River Laboratories in Canada (NIST SRM 4354);[39] and a soil material collected east of Helena, Montana (NIST SRM 2711a). These standards reflect challenging matrices for direct measurements with no prior chemical separation due to the relatively high metal content. Three aliquots of the standard solutions were then spiked to 0.05 pg/g of Pu, and another three aliquots were spiked to 0.05 pg/g Pu and 1 μg/g U for comparison.

Instrumentation. Analyses were performed by using an Agilent 8900 ICP-MS/MS (Agilent Technologies, Santa Clara, CA) instrument with NO as a reaction gas. The instrument is composed of a quadrupole mass filter preceding and following the CRC containing an octopole ion guide. The first quadrupole mass filter (Q1) resolves the ions before the CRC where it interacts with the collision/reaction gas. The octopole ion guide radially constrains the ions, minimizing the spreading of the beam as it propagates through the cell and ensuring efficient collection of product ions. Product and unreacted ions are subsequently mass resolved by the second quadrupole (Q2) and detected using a dual-mode electron multiplier detector. The instrument was equipped with a 100 $\mu L/min^{-1}$ microflow PFA nebulizer (Elemental Scientific, Omaha, NE) and a quartz double-pass spray chamber. The sample flow rate was optimized using a nebulizer and makeup gas flow rates to maximum sensitivity while minimizing plasma-derived oxides. The instrument used an integrated autosampler, s-lens, Ni sampler, and skimmer cones for most of the analyses. A c-lens was used instead of an s-lens during the actinide application measurements. MassHunter 4.6 Workstation Software (C.01.04) was used for instrument operation and data collection.

Reactivity scans were conducted mostly as described in previous investigations[5,6,11] using an ME standard at two NO flow rates (0.15 and 0.22 mL/min) at an octopole bias of −8

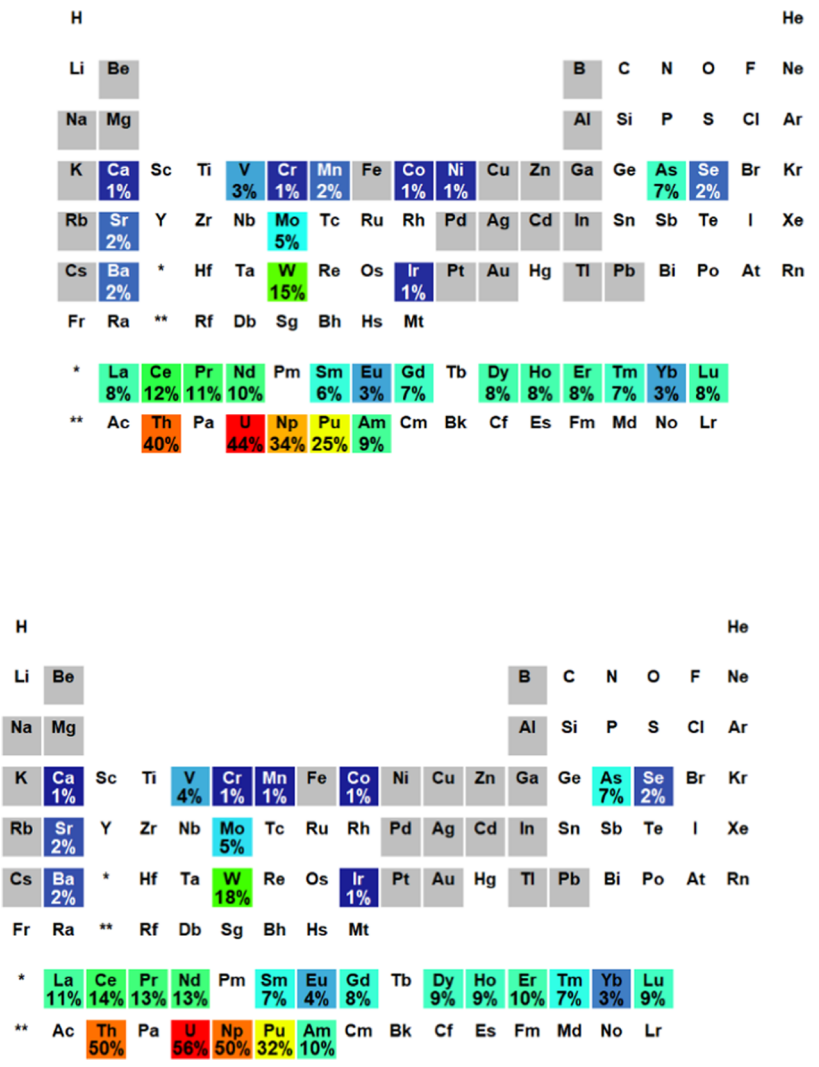

Figure 1. Percentage of MO^+ signal relative to the total signal intensities of all other ions containing M (M^+, MO^+, MN^+, and MO_2^+, etc.) at 0.15 (top) and 0.22 mL/min (bottom). Colors correspond to product species abundance: cool (blue) colors representing lower abundance than hot (red) colors. Elements colored gray were analyzed but reactivity was <1%. Unshaded elements were not measured.

V. Two flow rates are used to help determine the effect of increased pressure on product distribution. For this investigation, Q2 was set to the expected products (M^+, MN^+, MO^+, MNO^+, MO_2^+) instead of doing a full product mass scan to shorten analysis time. The investigation of polyatomic and isobaric interferences for actinide measurements using NO as the reaction gas in environmental samples followed a similar procedure. Instrument parameters for each experiment are listed in the Supporting Information (Table S1). The reactivities and backgrounds were characterized for Th^+, Np^+, U^+, UH^+, Pu^+, and Am^+ at three NO gas flows (0.15, 0.22, and 0.37 mL/min) with Q1 set to the m/z of M^+ and Q2 scanning from m/z of M^+ to m/z of 275 (maximum Q2 m/z on Agilent 8900). A NO flow rate of 0.37 mL/min was added to the actinide experiments due to this flow rate, providing the maximum sensitivity of Pu on the MO^+ product. For the remaining experiments, the Q2 product ions were focused on m/z M^+, MN^+, MO^+, MOH^+, MNO^+, MO_2^+, and MO_2H^+. Additional investigations were performed for the analysis of ^{239}Pu in the presence of ^{238}U creating $^{238}U^1H^+$ as an interfering ion. ^{239}Pu measurements of spiked NIST SRMs were analyzed with a NO flow rate of 0.37 mL/min with Q1 set to m/z = M and Q2 set to m/z = M, M + 15, and M + 16 which for Pu equates to Pu^+, PuO^+ and for U equates to UH^+, UO^+, and UOH^+.

RESULTS AND DISCUSSION

Product Ion Scans. *General Reactivity.* The primary product observed with NO as the reaction gas was MO^+ (Figure 1), with V, Cr, Co, As, Se, Mo, W, Ir, La, Ce, Pr, Nd, and Gd, forming a small amount of MN^+ product (<4%). No discernible change in the MN^+ product was observed at the higher gas flows (0.22 mL/min). Slight increases in MO^+ production were observed as the flow rate increased due to a higher probability of collisions in the CRC at the higher pressure. The MO^+ product formation was lower than that of N_2O, O_2, and CO_2,[5,6,40] likely due, in part, to the bond dissociation energy (BDE) of the reaction gases. The BDE for N−O is 6.5 eV, while for O═O, N_2−O, and OC═O, the BDE is 5.2, 1.7,[41] and 5.45 eV,[14] respectively. Trends in MO_2^+ formation for all three gases are similar to dioxide formation being greatest for N_2O, followed by CO_2, then NO.

In addition to elements analyzed by previous work,[5,6,11] general actinide reactivity was also assessed for Th^+, Np^+, U^+,

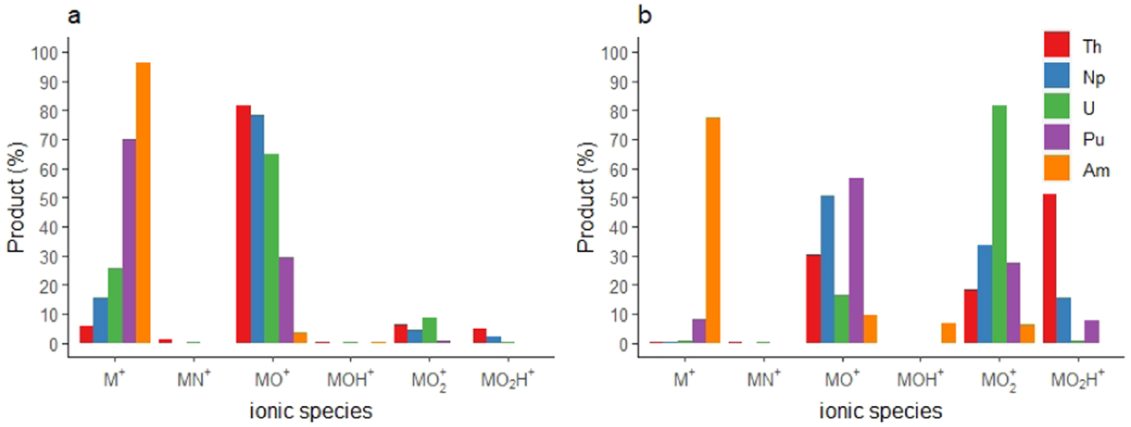

Figure 2. Percentage of ionic species formed relative to the total signal intensities of all other ions containing M (M^+, MO^+, MN^+, MO_2^+, etc.) at (a) 0.15 and (b) 0.37 mL/min.

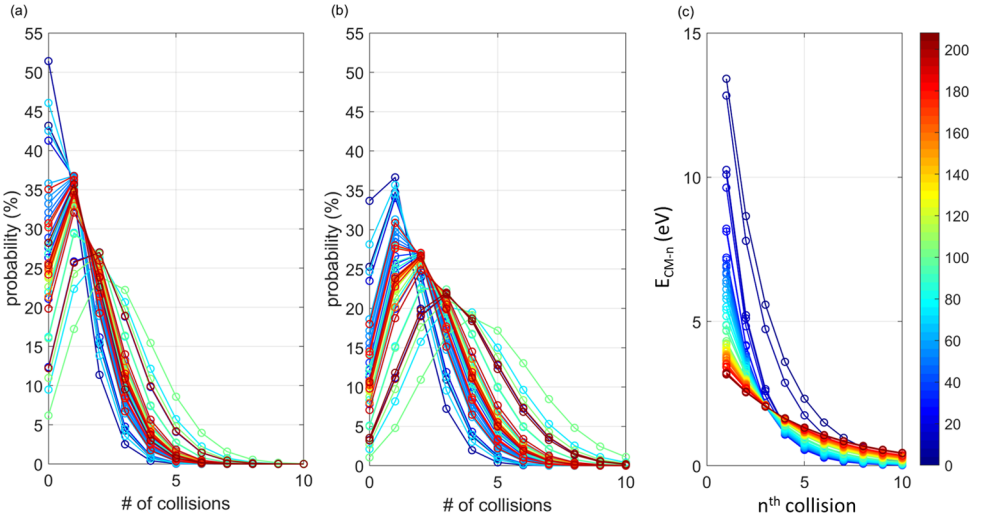

Figure 3. (a) The % probability of an ion of a given mass to experience up to 10 collisions at 0.15 mL/min, (b) up to 10 collisions at 0.22 mL/min, and (c) the kinetic energy of the ions upon encountering the *n*th collision. The colored bar indicates the analyte ion mass.

Pu^+, and Am^+ to determine trends in actinide reactivity and what product(s) might be useful for interference removal. Figure 2 shows the major products observed for all actinides analyzed at two gas flows (0.15 and 0.37 mL/min). The gas flow of 0.22 mL/min was omitted from Figure 2 for clarity; however, the reactivity was observed to be intermediate to the flow rates shown. Th^+, Np^+, and U^+ primarily formed MO^+ at 0.15 mL/min, while at the higher gas flow increased amounts of MO_2^+ were formed. Pu^+ was primarily unreactive with low MO^+ production at 0.15 mL/min, while at 0.37 mL/min, Pu^+ produced MO^+ and MO_2^+ with little remaining as M^+. Am^+ was the least reactive actinide with only 3.5% MO^+ production at 0.15 mL/min and 9.3% MO^+ and 6.4% MO_2^+ production at 0.37 mL/min. Additionally, MOH^+ was formed for Am (6.8%) and MO_2H^+ was formed for Th^+, Np^+, and Pu^+. Previous investigations also observed hydroxides formed for Pu^+ and Am^+ with NO as a reaction gas (Np^+ was not investigated previously).[24] The observed differences between Pu and Am may allow for isobaric separation of these elements (e.g., $^{241}Am/^{241}Pu$) using NO; however, this was not a focus of this study, so further investigation should be conducted in order to maximize the separation while also maintaining adequate sensitivity for both analytes.

DFT-Derived Reaction Enthalpies. Similar to previous studies,[5,6,11] characterization of the CRC was performed by calculating the laboratory frame energy (E_i), the energy available for reaction (E_{CM}), the probability an ion will experience a collision (P_n), and the ion energy at the most probable number of collisions ($E_{CM\text{-}j}$) with the neutral reaction gas. The probability of an ion undergoing *n* collisions at an NO flow of 0.15 and 0.22 mL/min and E_{CM} of the ion−molecule collision prior to *n* collisions are shown in Figure 3, Tables S2 and S3. The calculations indicate that most of the ions experience 0−1 collisions at an NO flow of 0.15 mL/min and 1−3 collisions at 0.22 mL/min. In previous work, we have utilized the energy (E_{CM}) of the ion after the most probable '*j*' number of collision, a rough approximation of the ions' average energy at reaction, to compare to the DFT modeled enthalpies; however, M^+ can have a distribution of collision energies that is important to consider when comparing $E_{CM\text{-}j}$ to the DFT-calculated ΔH.[11] This occurs because the energy model predicts the energy after a nonreactive collision, yet a reactive collision can occur whenever sufficient energy for a reaction to occur is available (see Supporting Information for additional details).[5,6,11]

DFT-calculated reaction enthalpies for oxide formation with NO are reported in Table S4. When available, the empirically

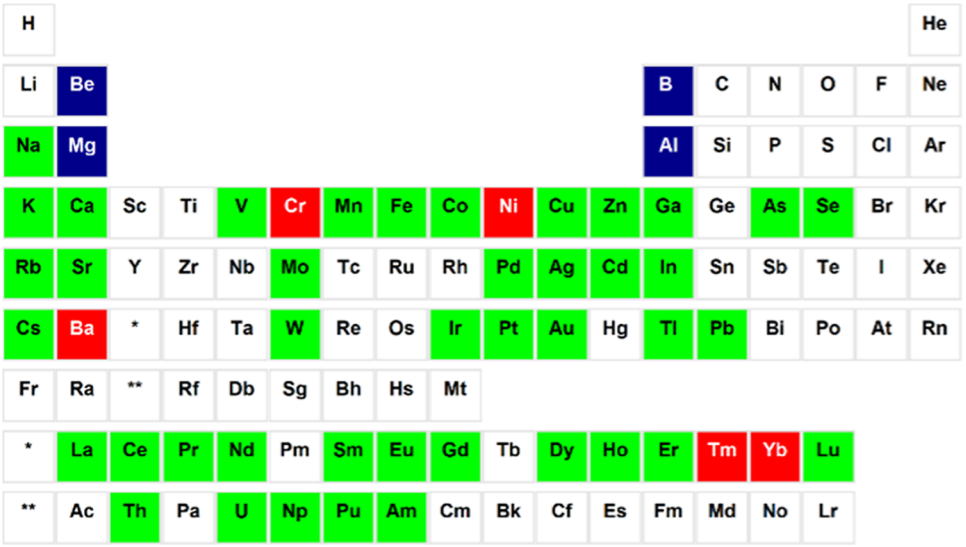

Figure 4. Accuracy of DFT-based predictions with elements that were accurately predicted to react (green), not predicted to react but a reaction was observed (red), and predicted to react but a reaction was not observed (blue).

measured reaction enthalpies from GIBMS experiments are also shown for comparison. DFT reaction enthalpies were compared to the calculated $E_{CM\text{-}j}$ (Tables S1 and S2) to predict which ions would react with NO (Figure 4). For the MO^+ product, the DFT-based predictions accurately predicted reaction outcomes for 82% of ions analyzed, where we define a reaction as having occurred if ≥1% product is observed in the total signal.

Elements that were not predicted to react, but a reaction was experimentally observed, include Cr^+, Ni^+, Ba^+, Tm^+, and Yb^+ (Figure 4). For these elements, the calculated enthalpies are similar to the expected available energy, and enough energy is present for the reaction to occur with the starting kinetic energy. Due to the distribution of ion energies present when entering the CRC, it is possible for the expected outcome to differ from what is observed experimentally, the closer $E_{CM\text{-}j}$ is to the DFT-derived ΔH. Further, the current energy model only calculates energy after nonreactive collisions so that if threshold requirements are met a reaction can occur at less than the most probable number of collisions.

Elements that were predicted to react, but a reaction was not experimentally observed, include Be^+, B^+, Mg^+, and Al^+. As reported for B^+ and Al^+ with OCS as the reaction gas,[11] barriers in excess of the reaction enthalpy have been observed for ground state ions with unfavorable electron configurations, and both B^+ and Al^+ are closed-shell ions (i.e., unfavorable electron configuration for reaction; $B^+ = [He]2s^2$; $Al^+ = [Ne]3s^2$) expected to be primarily in the ground state.[6,11,42] Another possible explanation is due to the high energy of the ion entering the cell; it is plausible for product dissociation to occur (i.e., $M^+ + NO \rightarrow M^+ + N + O$). Scattering outside the CRC may also explain the lack of an observed reaction for lighter elements as the lighter ions are rejected from the cell more easily than the heavier ions after colliding with the neutral gas. For NO, the Be^+ and B^+ had approximately 10% total ion transmission compared to the total ion transmission without gas in the CRC, while the heavier masses analyzed generally had >50% transmission. Overall, the DFT ΔH_{rxn} calculations are consistent with experimental observations for the ions analyzed (82% accuracy compared to $E_{CM\text{-}j}$ and 92% compared to the initial ion energy). This is less accurate for primary product prediction than previous work with CO_2, N_2O, and OCS;[5,6,11] however, this approach still provides a reasonable prediction of whether a reaction will occur when experimental data are not available.

In addition to using the DFT-calculated reaction enthalpies to understand when M^+ reacts, the reaction enthalpy was calculated for the reaction of NO with UH^+ to form MO^+ and MO_2^+, where ΔH_{rxn} was determined to be −2.2 eV (Table S4) and −9.1 eV, respectively. When comparing Pu^+ and UH^+ ΔH_{rxn}, PuO^+ is slightly endothermic (0.9 eV; Table S4) compared to the more favorable UH^+ reaction to either oxide product. The experimental data (Figure 5 and Table S4)

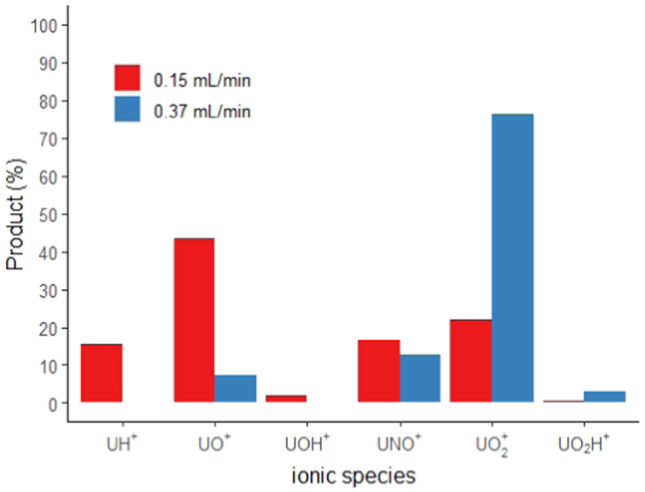

Figure 5. Percentage of ionic species formed from UH^+ relative to the total signal intensities of all other ions containing U (UO^+, UNO^+, UO_2^+, etc.) at 0.15 and 0.37 mL/min.

support the DFT calculations where the UH^+ ion is quite reactive and easily forms the oxide and dioxide products, with increasing dioxide formation with increasing gas flow. The MO_2^+ product requires at least two collisions to form; thus, at lower flow rates where fewer collisions are feasible (Figure 3), the primary product is UO^+ (Figure 5). When the gas flow is

Table 1. ^{239}Pu Concentration Measurements with and without Added ^{238}U[a]

		spiked standards				
SRM	n	[U] (ng/g soln)	[^{239}Pu] (pg/g soln)	^{239}Pu/^{238}U atomic ratio	[^{239}Pu] measured (pg/g soln)	error (%)
4354	4		0.047	3.59×10^{-5}	0.050 ± 0.003	5.4
4350b	4		0.046	1.98×10^{-5}	0.046 ± 0.002	−1.4
2711a	4		0.047	1.94×10^{-5}	0.047 ± 0.004	1.0
4354	4	1000	0.048	4.94×10^{-8}	0.051 ± 0.005	6.0
4350b	4	1000	0.046	4.74×10^{-8}	0.047 ± 0.004	1.1
2711a	4	1000	0.046	4.70×10^{-8}	0.045 ± 0.005	−1.1

[a]Uncertainties are 1σ. Error = $(V_{measured} - V_{known})/V_{known} \times 100$.

increased and the number of collisions subsequently increases (Figure 3), the primary product shifts to UO_2^+ (Figure 5) because it is the more enthalpically favorable product. Conversely, Pu^+ products are spread between the M^+, MO^+, and MO_2^+ products, especially at the higher gas flows. Enthalpically, the formation of UO_2^+ is very favorable so that at higher flow rates UO_2^+ is the predominate product. This enables Pu^+ analysis on the PuO^+ product. This is because two reactive collisions are required to form UO_2^+; thus, lower flow rates may show UO^+ as the primary product, because fewer collisions are probable. However, when the flow rate increases, UO_2^+ increases both because it is enthalpically favorable and the expected number of collisions has increased. Consequently, analyses were performed at a higher flow rate.

Application to Actinide Measurements. *^{239}Pu Interference Removal using ICP-MS/MS.* Typical interferences for $^{239}Pu^+$ measurements are peak tailing from $^{238}U^+$ and the polyatomic ions derived from matrix elements (e.g., $^{238}U^1H^+$, $^{207}Pb^{16}O_2^+$, $^{202}Hg^{37}Cl^+$, etc.) with the primary interference being $^{238}U^1H^+$, which is $\sim 10^{-5}$ relative to the $^{238}U^+$ signal using conventional ICP-MS.[43] Abundance sensitivity utilizing one quadrupole is typically $\sim 10^{-6}$, and the additional mass filter on ICP-MS/MS provides a theoretical abundance sensitivity of $\sim 10^{-12}$ that is beyond the dynamic range of the electron multiplier ($\sim 10^{11}$). Even so, the high abundance sensitivity essentially eliminates peak tailing interferences on m/z values of 237 and 239. Nonuranium-bearing polyatomic ions formed in the plasma from matrix components become a significant interference when measuring $^{239}Pu^+$ on mass in sample solutions with no pretreatment; therefore, ^{239}Pu was quantified using the $^{239}Pu^{16}O^+$ product at m/z 255 to mitigate these interferences.

The NO gas flow was increased to optimize the UH^+-Pu^+ separation which resulted in decreased MO^+ production and increased MO_2^+ production from UH^+ (Figure 5) and formation of MO^+ from Pu^+ (Table S5). This shift to higher-order products was larger for UH^+ relative to Pu^+, where increasing the NO gas flow from 0.15 to 0.37 mL/min resulted in an increase of 54.4% for UO_2^+ formation and 26.8% for PuO_2^+. UH^+ production of UOH^+, which would interfere with the analysis of $^{239}PuO^+$, decreased from 1.8 to 0.1% with an increased gas flow. Interestingly, UH^+ had slightly different reactivity compared to U^+ with UNO^+ forming at 12.8% (Figure 5). While the total ion transmission of Pu^+ (Pu^+, PuO^+, and PuO_2^+) decreased at the higher gas flow, the sensitivity of PuO^+ increased from 200 to 344 counts per second (CPS)/(pg/g). Increasing NO flow rates higher than 0.37 mL/min did improve interference removal but resulted in a reduced sensitivity of PuO^+ due to the increased formation of PuO_2^+ and transmission losses. Quantitative analysis of $^{239}Pu^+$ at the $^{239}PuO_2^+$ product was not achievable due to the elevated signals of $^{238}UO_2H^+$. Therefore, a NO flow of 0.37 mL/min was found to be the ideal balance between interference removal and the maximizing sensitivity for quantitation by "mass-shifting" to PuO^+.

The optimized tuning parameters gave a $^{238}U^{16}O^1H^+/^{238}U_{total}$ ratio of 8.8×10^{-8}, where $^{238}U^{16}O^1H^+$ is the contribution of UH^+ on the analyzed mass when Q1 is set to m/z 239 and $^{238}U_{total}$ is the intensity of all uranium containing product ions when Q1 is set to m/z 238. This method of calculating the interference ratio does not account for uranium product ions above an m/z of 275, which is the limit of the mass range of Q2 on Agilent 8900. Th, Np, Pu, and Am total ion transmission changed by <18% when increasing gas flow from 0.15 to 0.37 mL/min (Table SDATA1). Some amount of ion transmission loss is expected with increasing gas flows due to scatter, collisional dissociation, and energetic barriers. Conversely, U^+ exhibits an apparent 50% decrease in total ion transmission which we hypothesize is not an actual decrease in transmission but due to the formation of higher-order product species (>275 m/z). This indicates that the 8.8×10^{-8} interference ratio is likely a conservative upper limit for 0.37 mL/min NO as U_{total} would be underestimated. Previous literature[31,32] used the sensitivity of $^{238}U^+$ in MS/MS mode with 12 mL/min He for $^{238}U_{total}$. However, this method of calculating hydride removal does not account for ion transmission losses that occur when introducing reaction gases at higher flows.[33,35,36,44]

To show the utility of NO for $^{238}U^1H^+$ interference removal, various concentrations of ^{239}Pu (0.05−0.5 pg/g) were analyzed in a matrix containing 50−5000 ng/g of ^{238}U. Table S6 shows the determined concentrations of each solution analyzed, along with the ratio of Pu/U. All samples were quantitated using the $^{239}Pu^{16}O^+$ product ion. Ultimately, it was found that the background imparted by $^{238}U^{16}O^1H^+$ was ~0.04 CPS/(ng/g) ^{238}U (Table S5). Given a $^{239}Pu^{16}O$ sensitivity of 3.4×10^5 CPS/(ng/g), the $^{238}U^{16}O^1H^+$ background contribution to the $^{239}Pu^{16}O$ signal is minimal; however, a correction was performed to determine an accurate ^{239}Pu concentration in samples where the Pu/U ratio is $< 5 \times 10^{-7}$. The corrected concentrations containing >100 ng/g ^{238}U show good agreement with the true sample concentration with all ^{239}Pu measurements within 10% error. The advantage to this method when compared to CO_2[31,37] and O_2[32] as the reaction gas is that ^{239}Pu is mass-shifted away from both the matrix ($^{239}Pu^+$ to $^{239}Pu^{16}O^+$) and the primary interference ion ($^{238}U^1H^+$ to $^{238}UO_2^+$).

Determination of ^{239}Pu in Spiked Standard Reference Material. Three certified reference material (SRM 4354, 4350b, and 2711a) solutions were spiked with 0.05 pg/g

^{239}Pu, and an aliquot of the solutions was spiked with 1000 ng/g ^{238}U to determine how this in-line separation method performs in a high matrix sample containing significant levels of U. The on-mass intensity in the unspiked aliquot for m/z 239 was ∼30 CPS for SRM 2711a and was at background levels (<1 CPS) for SRM 4354 and 4350b. The increased backgrounds observed in SRM 2711a are likely from the high levels of Pb (0.14%) present in the soil, resulting in $^{207}Pb^{16}O_2^+$ interferences. As mentioned previously, $^{239}Pu^+$ was measured at m/z 255 ($^{239}Pu^{16}O^+$) for quantitation to avoid such polyatomic interferences. The analytical results (Table 1) show that all spiked SRMs measured were within a 6% error of the correct value regardless of the amount of uranium in the solution. The relative standard uncertainty was ∼10% for the standard spiked with just ^{239}Pu and increased to ∼17% for the standards spiked with uranium due to the contribution of uncertainty from the hydride correction. The limit of detection (LOD), calculated using 3 times the standard deviation of the reagent blanks (n = 3), for the ^{239}Pu measurements with SRMs not spiked with ^{238}U was 0.18 fg/g of solution (170 fg/g of soil). The SRM aliquots that were spiked with uranium had an LOD of 3.9 fg/g of solution (3.8 pg/g of soil), which was estimated from the standard deviation of the $^{238}U^{16}O^1H^+/^{238}U^{16}O^+$ ratio measured in the 400 ng/g U standard solution that is used to obtain the correction (eq S1).

CONCLUSIONS

Gas-phase ion reactivity of NO was assessed using ICP-MS/MS for 50 elements including Th, Np, U, Pu, and Am. MO^+ was the primary product observed across the elements analyzed. Reaction enthalpies were calculated using the DFT model with 82% accuracy in predicting MO^+ reactivity when compared to the observed reaction at $E_{CM\text{-}j}$. To demonstrate the top-down approach using DFT to guide analyses, the reaction enthalpy of $^{238}U^1H$ was also calculated and compared to provide an initial prediction of the feasibility to remove this polyatomic interference for ^{239}Pu analysis. This work demonstrates that initial knowledge of reactivity from theoretical calculations can guide method development for the removal of isobaric interferences (including polyatomic interferences generated in the plasma) for a variety of practical applications.

This work demonstrates a novel method to measure actinides in the presence of the sample matrix without the need for extensive analyte separation and is the first to show the feasibility of using NO as the reaction gas for actinide analyses. Measured ^{239}Pu concentrations were determined to be within 6% of the spiked value in environmental samples, at all levels of U tested. The background contribution from $^{238}U^1H^+$ was decreased to 8.8×10^{-8} (or 0.04 CPS/(ng/g)) and, because ^{239}Pu was analyzed at the oxide, polyatomic interferences from other matrix elements (e.g., $^{207}Pb^{16}O_2^+$, $^{202}Hg^{37}Cl^+$, etc.) were eliminated. The developed method has ^{239}Pu LODs of 0.18 fg/g of solution in samples containing 1 ng/g of ^{238}U and 3.9 fg/g of solution in samples containing 1 ug/g of ^{238}U. The reactivity of Th, Np, and Am was also investigated with NO that, to the best of our knowledge, has not been presented elsewhere. The observed reactivity with NO demonstrates that the long-lived actinide isotopes (e.g., ^{232}Th, ^{238}U, ^{239}Pu, ^{237}Np, and ^{243}Am) can be measured during the same analysis for complex environmental samples relevant to nuclear forensics.

ASSOCIATED CONTENT

Expansion on previous fundamental studies, energy calculations, and graphs for the probability of collisions and the resulting energy after collision, computational details, uranium hydride correction calculation, calculated reaction enthalpies, signal intensities and percent product formation from actinide reactivity experiments, and ^{239}Pu determinations made in a multielement standard of U and Pu (PDF)

AUTHOR INFORMATION

Corresponding Author

Amanda D. French − *Pacific Northwest National Laboratory, Richland, Washington 99352, United States;* orcid.org/0000-0002-8417-6091; Email: Amanda.French@pnnl.gov

Authors

Kirby P. Hobbs − *Pacific Northwest National Laboratory, Richland, Washington 99352, United States;* orcid.org/0009-0004-8537-2811

Kali M. Melby − *Pacific Northwest National Laboratory, Richland, Washington 99352, United States*

Eric J. Bylaska − *Pacific Northwest National Laboratory, Richland, Washington 99352, United States;* orcid.org/0000-0001-6405-599X

Khadouja Harouaka − *Pacific Northwest National Laboratory, Richland, Washington 99352, United States;* orcid.org/0000-0002-5305-0138

Richard M Cox − *Pacific Northwest National Laboratory, Richland, Washington 99352, United States;* orcid.org/0000-0003-1812-3431

Isaac J. Arnquist − *Pacific Northwest National Laboratory, Richland, Washington 99352, United States*

Chelsie L. Beck − *Pacific Northwest National Laboratory, Richland, Washington 99352, United States;* orcid.org/0000-0002-5958-451X

Notes

The authors declare no competing financial interest.

ACKNOWLEDGMENTS

This work was funded by PNNL's Laboratory Directed Research and Development program under the m/q Initiative, the Office of Defense Nuclear Nonproliferation Research and Development within the U.S. Department of Energy's National Nuclear Security Administration, and the Office of the Deputy Assistant Secretary of Defense for Nuclear Matters. The Pacific Northwest National Laboratory is a multiprogram national laboratory operated for the U.S. Department of Energy (DOE) by Battelle Memorial Institute under contract number DE-AC05-76RL01830.

REFERENCES

(1) Ohno, T.; Muramatsu, Y.; Shikamori, Y.; Toyama, C.; Okabe, N.; Matsuzaki, H. *J. Anal. At. Spectrom.* **2013**, *28* (8), 1283−1287.

(2) Eiden, G. C.; Barinaga, C. J.; Koppenaal, D. W. *Rapid Commun. Mass Spectrom.* **1997**, *11* (1), 37−42.

(3) Harouaka, K.; Hoppe, E. W.; Arnquist, I. J. *J. Anal. At. Spectrom.* **2020**, *35* (12), 2859−2866.
(4) Balcaen, L.; Bolea-Fernandez, E.; Resano, M.; Vanhaecke, F. *Anal. Chim. Acta* **2015**, *894*, 7−19.
(5) Harouaka, K.; Allen, C.; Bylaska, E.; Cox, R. M.; Eiden, G. C.; di Vacri, M. L.; Hoppe, E. W.; Arnquist, I. J. *Spectrochim. Acta, Part B* **2021**, *186*, No. 106309.
(6) Harouaka, K.; Melby, K.; Bylaska, E. J.; Cox, R. M.; Eiden, G. C.; French, A.; Hoppe, E. W.; Arnquist, I. J. *Geostand. Geoanal. Res.* **2022**, *46* (3), 387−399.
(7) Balcaen, L.; Woods, G.; Resano, M.; Vanhaecke, F. *J. Anal. At. Spectrom.* **2013**, *28* (1), 33−39.
(8) Bolea-Fernandez, E.; Balcaen, L.; Resano, M.; Vanhaecke, F. *J. Anal. At. Spectrom.* **2016**, *31* (1), 303−310.
(9) Bolea-Fernandez, E.; Balcaen, L.; Resano, M.; Vanhaecke, F. *Anal. Chem.* **2014**, *86* (15), 7969−7977.
(10) Zhu, Y. *Chem. Lett.* **2018**, *47* (6), 740−743.
(11) French, A. D.; Melby, K. M.; Cox, R. M.; Bylaska, E.; Eiden, G. C.; Hoppe, E. W.; Arnquist, I. J.; Harouaka, K. *Spectrochim. Acta, Part B* **2023**, *207*, No. 106754.
(12) Diez-Fernández, S.; Isnard, H.; Nonell, A.; Bresson, C.; Chartier, F. *J. Anal. At. Spectrom.* **2020**, *35* (12), 2793−2819.
(13) Cox, R. M.; Melby, K. M.; French, A. D.; Rodriguez, M. J. *Phys. Chem. Chem. Phys.* **2023**, *26* (1), 209−218.
(14) Cox, R. M.; Harouaka, K.; Citir, M.; Armentrout, P. B. *Inorg. Chem.* **2022**, *61* (21), 8168−8181.
(15) Blagojevic, V.; Flaim, E.; Jarvis, M. J. Y.; Koyanagi, G. K.; Bohme, D. K. *J. Phys. Chem. A* **2005**, *109* (49), 11224−11235.
(16) Blagojevic, V.; Flaim, E.; Jarvis, M. J. Y.; Koyanagi, G. K.; Bohme, D. K. *Int. J. Mass Spectrom.* **2006**, *249*−*250*, 385−391.
(17) Cox, R. M.; Kafle, A.; Armentrout, P. B.; Peterson, K. A. *J. Chem. Phys.* **2019**, *151* (3), No. 034304.
(18) Khan, F. A.; Steele, D. L.; Armentrout, P. B. *J. Phys. Chem. A* **1995**, *99* (19), 7819−7828.
(19) Rodgers, M. T.; Walker, B.; Armentrout, P. B. *Int. J. Mass Spectrom.* **1999**, *182*−*183*, 99−120.
(20) Gibson, J. K.; Haire, R. G.; Marçalo, J.; Santos, M.; Leal, J. P.; Pires de Matos, A.; Tyagi, R.; Mrozik, M. K.; Pitzer, R. M.; Bursten, B. E. *Eur. Phys. J. D* **2007**, *45* (1), 133−138.
(21) Gibson, J. K.; Haire, R. G.; Santos, M.; Marçalo, J.; Pires de Matos, A. *J. Phys. Chem. A* **2005**, *109* (12), 2768−2781.
(22) Santos, M.; Marçalo, J.; Leal, J. P.; Pires de Matos, A.; Gibson, J. K.; Haire, R. G. *Int. J. Mass Spectrom.* **2003**, *228* (2), 457−465.
(23) Santos, M.; Marçalo, J.; Pires de Matos, A.; Gibson, J. K.; Haire, R. G. *J. Phys. Chem. A* **2002**, *106* (31), 7190−7194.
(24) Matsueda, M.; Kawakami, T.; Koarai, K.; Terashima, M.; Fujiwara, K.; Iijima, K.; Furukawa, M.; Takagai, Y. *Chem. Lett.* **2022**, *51* (7), 678−682.
(25) Tanner, S. D.; Li, C.; Vais, V.; Baranov, V. I.; Bandura, D. R. *Anal. Chem.* **2004**, *76* (11), 3042−3048.
(26) Crain, J. S.; Smith, L. L.; Yaeger, J. S.; Alvarado, J. A. *J. Radioanal. Nucl. Chem.* **1995**, *194* (1), 133−139.
(27) Pointurier, F.; Hémet, P.; Hubert, A. *J. Anal. At. Spectrom.* **2008**, *23* (1), 94−102.
(28) Kishimoto, T.; Sanada, T.; Sato, K.; Higuchi, H. *J. Radioanal. Nucl. Chem.* **2002**, *252* (2), 395−398.
(29) Pointurier, F.; Hubert, A.; Fauré, A.-L.; Hémet, P.; Pottin, A.-C. *J. Anal. At. Spectrom.* **2011**, *26* (7), 1474−1480.
(30) Xing, S.; Zhang, W.; Qiao, J.; Hou, X. *Talanta* **2018**, *187*, 357−364.
(31) Hou, X.; Zhang, W.; Wang, Y. *Anal. Chem.* **2019**, *91* (18), 11553−11561.
(32) Zhang, W.; Lin, J.; Fang, S.; Li, C.; Yi, X.; Hou, X.; Chen, N.; Zhang, H.; Xu, Y.; Dang, H.; et al. *Talanta* **2021**, *234*, No. 122652.
(33) Ni, Y.; Bu, W.; Xiong, K.; Hu, S.; Yang, C.; Cao, L. *Talanta* **2023**, *262*, No. 124710.
(34) Olufson, K. P.; Moran, G. *J. Radioanal. Nucl. Chem.* **2016**, *308* (2), 639−647.
(35) Diez-Fernández, S.; Jaegler, H.; Bresson, C.; Chartier, F.; Evrard, O.; Hubert, A.; Nonell, A.; Pointurier, F.; Isnard, H. *Talanta* **2020**, *206*, No. 120221.
(36) Jaegler, H.; Gourgiotis, A.; Steier, P.; Golser, R.; Diez, O.; Cazala, C. *Anal. Chem.* **2020**, *92* (11), 7869−7876.
(37) Tiong, L. Y. D.; Tan, S. *J. Radioanal. Nucl. Chem.* **2019**, *322* (2), 399−406.
(38) Savina, M. R.; Shulaker, D. Z.; Isselhardt, B. H.; Brennecka, G. A. *J. Anal. At. Spectrom.* **2023**, *38* (6), 1205−1212.
(39) Goldstein, S. J.; Price, A. A.; Hinrichs, K. A.; Lamont, S. P.; Nunn, A. J.; Amato, R. S.; Cardon, A. M.; Gurganus, D. W. *J. Environ. Radioact.* **2021**, *237*, No. 106689.
(40) Sugiyama, N.; Nakano, K. *Reaction Data for 70 Elements using O2, NH3 and H2 gases with the Agilent 8800 Triple Quadrupole ICP-MS*; Application Note, 5991−4585ENAgilent Technologies Inc., 2014.
(41) Armentrout, P. B.; Halle, L. F.; Beauchamp, J. L. *J. Chem. Phys.* **1982**, *76* (5), 2449−2457.
(42) Armentrout, P. B.; Cox, R. M. *Phys. Chem. Chem. Phys.* **2017**, *19* (18), 11075−11088.
(43) Tanimizu, M.; Sugiyama, N.; Ponzevera, E.; Bayon, G. *J. Anal. At. Spectrom.* **2013**, *28* (9), 1372−1376.
(44) Russell, B. C.; Warwick, P. E.; Mohamud, H.; Pearson, O.; Yu, Y.; Thompkins, H.; Goddard, S. L.; Croudace, I. W.; Zacharauskas, Z. *J. Anal. At. Spectrom.* **2023**, *38* (1), 97−110.